The Role of Reversed Equatorial Zonal Transport in Terminating an ENSO Event

HAN-CHING CHEN

Department of Atmospheric Sciences, National Taiwan University, Taipei, Taiwan, and Department of Atmospheric, Oceanic and Earth Sciences, College of Science, George Mason University, Fairfax, Virginia

ZENG-ZHEN HU

NOAA/NWS/NCEP/Climate Prediction Center, College Park, Maryland

BOHUA HUANG

Department of Atmospheric, Oceanic and Earth Sciences, College of Science, George Mason University, Fairfax, Virginia

CHUNG-HSIUNG SUI

Department of Atmospheric Sciences, National Taiwan University, Taipei, Taiwan

(Manuscript received 5 January 2016, in final form 7 May 2016)

ABSTRACT

This study shows the sudden basinwide reversal of anomalous equatorial zonal transport above the thermocline at the peaking phase of ENSO triggers rapid termination of ENSO events. The anomalous equatorial zonal transport is controlled by the concavity of anomalous thermocline meridional structure across the equator. During the developing phase of ENSO, opposite zonal transport anomalies form in the western-central and central-eastern equatorial Pacific, respectively. Both are driven by the equatorial thermocline anomalies in response to zonal wind anomalies over the western-central equatorial ocean. At this stage, the anomalous zonal transport in the east enhances ENSO growth through zonal SST advection. In the mature phase of ENSO, off-equatorial thermocline depth anomalies become more dominant in the eastern Pacific because of the reflection of equatorial signals at the eastern boundary. As a result, the meridional concavity of the thermocline anomalies is reversed in the east. This change reverses zonal transport rapidly in the central-to-eastern equatorial Pacific, joining with the existing reversed zonal transport anomalies farther to the west, and forms a basinwide transport reversal throughout the equatorial Pacific. This basinwide transport reversal weakens the ENSO SST anomalies by reversed advection. More importantly, the reversed zonal transport reduces the existing zonal tilting of the equatorial thermocline and weakens its feedback to wind anomalies effectively. This basinwide reversal is built in at the peak phase of ENSO as an oceanic control on the evolution of both El Niño and La Niña events. The reversed zonal transport anomaly after the mature phase weakens El Niño in the eastern Pacific more efficiently than it weakens La Niña.

1. Introduction

The El Niño–Southern Oscillation (ENSO) phenomenon is a Pacific basinwide interannual variation of the tropical ocean–atmosphere system. ENSO is generally characterized as an oscillation of 3–7 years, and major warm and cold ENSO episodes (i.e., El Niños and La Niñas) evolve as distinctive events that usually last for about one year, with intensive anomalies of the sea surface temperature (SST) initiating in boreal spring, growing in summer and fall, peaking in winter, and then decaying in the next spring. It has long been recognized that the growth of an ENSO cycle is due to the positive dynamical feedback among the equatorial SST, wind stress, and the zonal slope of thermocline, known as the

Corresponding author address: Han-Ching Chen, Department of Atmospheric Sciences, National Taiwan University, Taipei 10617, Taiwan.
E-mail: d00229002@ntu.edu.tw

DOI: 10.1175/JCLI-D-16-0047.1

Bjerknes feedback (Bjerknes 1969). However, what processes cause an equally fast termination of an ENSO event, when a peaking El Niño quickly dissipates in spring and sometimes turns into a La Niña by summer, is less well explained.

The termination of ENSO events is usually examined in the framework of phase transition within an ENSO cycle. Several conceptual ENSO models have proposed different delayed negative feedbacks that are necessary to sustain the coupled oscillation. 1) The "delayed oscillator" theory (Suarez and Schopf 1988; Battisti and Hirst 1989) suggested that the delayed negative feedback is caused by off-equatorial Rossby wave signals with the opposite sign to an ongoing ENSO event. These Rossby wave signals are generated by the wind anomalies in the equatorial Pacific, which propagate to the western boundary and are reflected as equatorial Kelvin waves to decay the SST anomalies in the eastern Pacific. 2) The early idea of Wyrtki (1985) showed that the warm water of the western Pacific tends to increase prior to an El Niño event, and then decreases during the process of the event. Jin (1997a,b) and Li (1997) proposed a "recharge–discharge oscillator" scenario to describe how the warm water volume (WWV) could facilitate the transition of ENSO event. 3) The "western Pacific oscillator" model developed by Weisberg and Wang (1997) emphasizes the role of off-equatorial SST anomalies in the western Pacific, which induce equatorial wind anomalies there and generate the Kelvin wave signal as a negative feedback to reverse the phase of ENSO. 4) Picaut et al. (1997) proposed an "advective–reflective oscillator" model through observational analyses. This conceptual model emphasized the importance of zonal advection of the mean SST by anomalous zonal current associated with the wave reflections at the eastern and western boundaries of the Pacific Ocean. The negative feedback forces the coupled ocean–atmosphere system to oscillate. A unified oscillator model has been developed based on the physics of the above delayed negative feedback mechanisms (Wang 2001). In this general framework, all of the four mechanisms discussed above can be seen as special cases of the unified oscillator model. The unified oscillator demonstrates that ENSO is a multimechanism phenomenon and the relative importance of different mechanisms is time dependent. As a result, it provides a more comprehensive description of the physical mechanisms of the ENSO cycle than each of the mechanisms alone.

However, it is not clear whether these negative feedback mechanisms, some of which emphasize the gradual phase transition within a low-frequency ENSO cycle, could adequately explain the more sudden termination of an ENSO event, compared with its growth. For instance, in the conceptual model developed by Jin (1997a), the zonally averaged recharge–discharge process seems to have no direct influence on the zonal thermocline slope, because the latter is assumed to be in balance with the zonally averaged wind stress anomalies instead of the meridional heat exchange between the equator and areas off the equator (e.g., Schneider et al. 1995). As a result, the recharge–discharge process is unlikely to be the main factor that stops the unstable ENSO growth and terminate ENSO event suddenly. For the delayed oscillator, although there is substantial evidence of western boundary reflection (e.g., Mantua and Battisti 1994; Zang et al. 2002), over 80% of equatorial Kelvin waves in the central Pacific are forced by winds (Boulanger et al. 2003). For example, at the end of the 1997/98 El Niño, upwelling Kelvin-wave signals are mostly generated by easterly wind anomalies (Weisberg and Wang 1997; Wang et al. 1999; McPhaden and Yu 1999; Boulanger and Menkes 2001). There seems no concrete evidence that a reflected signal can propagate as an uncoupled Kelvin wave into the eastern equatorial Pacific. The coupled equatorial propagation seems much slower (Cai 2003).

Some studies have suggested that a meridional shift of the surface zonal westerly wind anomalies from the equator to the Southern Hemisphere in boreal winter is responsible for the quick termination of El Niño events (Harrison 1987; Harrison and Vecchi 1999; Larkin and Harrison 2002; Vecchi and Harrison 2003; Lengaigne et al. 2006). At the peak of an El Niño event, such southward wind shift weakens the equatorial westerly anomalies and generates eastward propagating upwelling Kelvin waves. This process is similar to that proposed by Weisberg and Wang (1997), except that the wind shift is argued to be driven by the southward displacement of the warmest water, following the seasonal march (e.g., Spencer 2004; Lengaigne et al. 2006). This interaction between the ENSO low-frequency component and the western Pacific annual cycle not only explains the sudden change in this phase of ENSO evolution but also accounts for the ENSO phase lock with the seasonal cycle naturally (Stuecker et al. 2013). However, the effect of southward wind shift seems to be limited to El Niño events. According to Zhang et al. (2015), there is no distinct southward wind displacement over the central Pacific during decaying phase of La Niña. Furthermore, although earlier studies (e.g., Harrison and Larkin 1998) suggested that the central equatorial Pacific westerly wind anomalies move south of the equator in the winter of every El Niño, more recent studies (e.g., Stuecker et al. 2013) argue that this process occurs much more prominently for strong El Niño than for weak El Niño. Zhang et al. (2015) also showed that the wind shift appears only during eastern-Pacific El Niño events rather than during central-Pacific El Niño events,

which is probably also related to their different strengths. Whether wind shift is a universal mechanism of ENSO termination still needs investigation.

In this paper, we demonstrate that a sudden basinwide reversal of the zonal equatorial current at the peaking phase of ENSO may be a trigger to the rapid termination of an ENSO event. This mechanism is dependent upon the fact that the equatorial zonal current is controlled by the relative strength of the equatorial and off-equatorial thermocline anomalies through geostrophic balance. During the developing phase of ENSO, the zonal current is driven by equatorial thermocline anomalies. As a result, thermocline anomalies forced by equatorial zonal wind anomalies over the western-central Pacific generate opposite zonal current anomalies locally and to the east. The latter enhances the ENSO growth through zonal SST advection. In the mature phase of ENSO, because the thermocline depth anomalies are reflected in the eastern Pacific and propagate westward in both hemispheres, the off-equatorial thermocline depth anomalies become higher than that on the equator for El Niño events and lower for La Niño events. Combined with the existing zonal current anomalies in the western-central Pacific, this meridional structure change of thermocline reverses zonal transport throughout the equatorial Pacific. The reversed zonal transport in the mature phase can rapidly weaken the ENSO amplitude by reversing the temperature advection. More importantly, this reversal changes the mass balance in the eastern equatorial Pacific that weakens the existing zonal tilting of equatorial thermocline. Both processes are concentrated in the eastern equatorial Pacific and can be effective on seasonal time scales. Overall, the current reversal mechanism is built in to the peak phase of ENSO in both El Niño and La Niña.

The wave reflection at the eastern boundary discussed in the advective–reflective oscillator (Picaut et al. 1997) may play a major role in the current reversal. However, we argue that the basinwide character of current reversal is due to not only eastern boundary reflection but also the wind-driven current farther to the west. Both factors can be represented by the concavity of meridional thermocline anomalies, simpler than projecting to wave modes (e.g., Boulanger and Menkes 1999). Like Jin and An (1999), we also link the zonal advective feedback with thermocline feedback via geostrophic balance. However, we emphasize that these two processes are not in phase after the current reversal. Another distinction between our study and the previous ones is that we not only invoke zonal current as a mechanism for SST advection but also consider its direct effects on mass balance.

The rest of the paper is structured as follows. Section 2 describes the datasets and the methods used in this paper. Section 3 describes the general evolution of the typical El Niño and La Niña events in the equatorial Pacific. Section 4 discusses the roles played by both the zonal and meridional transports during the evolution and the physical processes that generate these anomalous currents. Finally, a summary and discussion is given in section 5.

2. Data

Monthly means of 20°C isotherm depth (D20) and ocean current on a 0.333° latitude × 1.0° longitude global grid are from the Global Ocean Data Assimilation System (GODAS; Behringer and Xue 2004). D20 is generally used as an indicator for the tropical thermocline depth. Therefore, the ocean mass transport above the thermocline is defined in this study as transport integrated vertically from the surface to D20. The SST dataset used in this study is the monthly HadISST data on a 1° × 1° grid (Rayner et al. 2003), which is a long-term global SST analysis available from 1870 to the present. It is based on historical in situ ship and buoy observations with satellite data blended in after 1982. The cold bias of bucket SST measurements prior to 1942 is corrected and missing grids are filled by optimal interpolation based on EOF analysis. The surface wind data (0.995 sigma level) from the National Centers for Environmental Prediction–National Center for Atmospheric Research (NCEP–NCAR) reanalysis project (Kalnay et al. 1996; Kistler et al. 2001) on a 2.5° × 2.5° grid is used to analyze the corresponding ocean–atmosphere interaction. Because GODAS output starts from 1980, we analyze all the output from 1980 to 2015 in this study.

The selection of ENSO events follows the ENSO year definition by the Climate Prediction Center of NOAA based on the Niño-3.4 index (http://www.cpc.ncep.noaa.gov/products/analysis_monitoring/ensostuff/ensoyears.shtml). Only moderate and strong El Niño and La Niña events with five consecutive overlapping 3-month mean Niño-3.4 SSTA at or above 1.0°C are used in the composite analysis of this study. We exclude the events in 1987/88 because this event follows a strong El Niño and does not reach its peak intensity near boreal winter. During the analysis period, there were six El Niño events (1982/83, 1986/87, 1991/92, 1997/98, 2002/03, and 2009/10) and five La Niña events (1988/89, 1998/99, 1999/00, 2007/08, and 2010/11). A composite El Niño (La Niña) event is defined as the average of the corresponding calendar months of all El Niño (La Niña) events for a maximum of 3-yr duration, starting from the

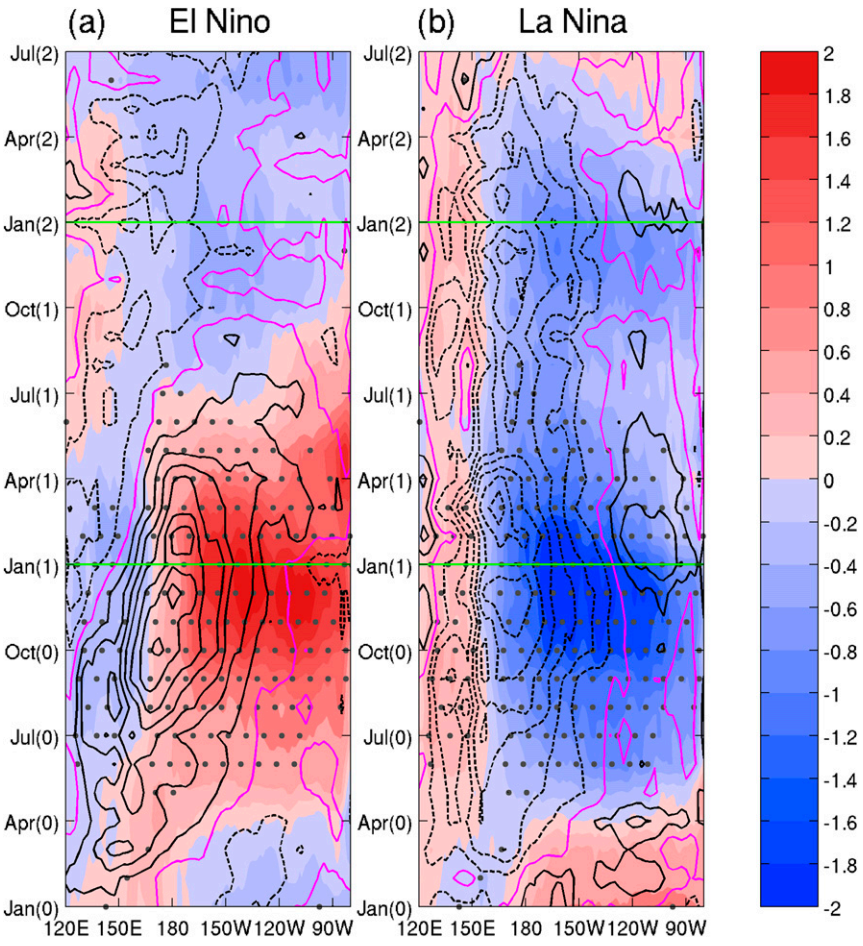

FIG. 1. Hovmöller diagram of SST (shading) and zonal surface wind (contour) anomalies averaged between 5°S and 5°N for composite of (a) El Niño and (b) La Niña years. The purple lines represent zero wind anomalies, with solid (dashed) lines for positive (negative) surface wind anomalies. The gray dots indicate the difference of SST between El Niño and La Niña exceeding a 95% confidence level using a *t* test. The contour interval is 0.4 m s^{-1} for wind anomalies and shading interval is 0.2°C for SST anomalies. The green lines represent January of Year(1) and Year(2), respectively.

developing year [Year(0)] to decaying year [Year(1)] and afterward [Year(2)].

3. Equatorial evolution of El Niño and La Niña events

We first present the general life cycle of the composite warm and cold ENSO events to establish their major characteristics. Figure 1 shows the composite evolution of SST (shading) and zonal surface wind (contour) anomalies along the equator during El Niño and La Niña. For El Niño (Fig. 1a), the positive SST anomalies are initiated in the western Pacific in Year(0) and propagate eastward to the central and eastern Pacific. For La Niña (Fig. 1b), however, the negative SST anomalies occur simultaneously across the basin since the early summer of Year(0). The evolutions of the SST anomalies show a physically consistent pattern with zonal surface wind anomalies over the equatorial Pacific: the peak of westerly (easterly) wind anomaly is collocated with minimum (maximum) zonal gradients of SST anomalies. This wind–SST anomaly collocation suggests that the SST and surface wind anomalies are amplified through the Bjerknes air–sea interaction in the central and eastern equatorial Pacific (Bjerknes 1969) and reach their peaks around the winter of Year(0)–Year(1). During the mature phase, the negative SST anomalies for La Niña extend farther west in the western Pacific compared to the positive SST anomalies for El Niño. The associated surface wind anomalies extend farther

westward in La Niña compared to El Niño. This difference is mainly associated with the fact that the zonal wind anomalies migrate eastward from Jun(0) to Apr(1)—note that months will be referred to by their first three letters: Jan, Feb, etc.)—the during the El Niño event (contours, Fig. 1a), while the wind anomalies remain stationary in the same period during the La Niña event (contours, Fig. 1b).

After the mature phase, the negative SST anomalies for the El Niño event start to propagate eastward in May(1), associated with the weakening of the westerly wind anomalies over the central Pacific and an eastward migration of the easterly wind anomalies from farther west (Fig. 1a). As the cold SST anomalies move into the central Pacific in the summer of Year(1), the El Niño event is ended and the eastern equatorial Pacific turns into a cold episode. For the La Niña, however, the positive SST anomalies remain stationary in the western equatorial Pacific throughout Year(0) to Year(1) without any propagation (shading, Fig. 1b). The cold SST and easterly wind stress anomalies in the central Pacific also remain stationary throughout Year(1) and the spring of Year(2). Farther to the east, associated with the appearance of weak westerly wind anomalies between 90° and 120°W in early Year(1), the cold SST anomalies weaken temporarily from Jan(1) to Jul(1). However, the cold SST anomalies recover in the eastern Pacific during the latter half of Year(1) and occur a secondary peak in early Year(2), before finally dissipating in the late spring of Year(2).

The evolution of the equatorial thermocline depth anomalies is crucial to explain the ENSO development and phase transition. The contour in Fig. 2 shows the composite evolution of D20 anomalies averaged in 5°N and 5°S during El Niño and La Niña. According to these composites, the D20 anomalies are initiated in the western Pacific in Year(0) during both the El Niño and La Niña years, and then propagate eastward. As documented by Schneider et al. (1995), the slope of the equatorial thermocline anomalies is proportional to the surface wind. During the winter of Year(0)–Year(1), the deepening or shallowing of the thermocline in the eastern Pacific is collocated with the major SST anomalies, manifesting the subsurface component of the positive ocean–atmosphere feedback process (Bjerknes feedback) that brings El Niño or La Niña event to a mature phase. For the transition of both events, opposite D20 anomalies start to propagate slowly eastward starting from Jul(0). For El Niño, the negative D20 anomalies (contour, Fig. 2a) propagate roughly at the same pace as that of the surface wind anomalies (contour, Fig. 1a), reaching the eastern boundary around Jul(1). For La Niña, however, the eastward migration of the positive D20 anomalies stops at the central Pacific in Jan(1) (contour, Fig. 2b). It is noticeable, however, that a mild positive D20 anomaly appears in the eastern Pacific from Apr(1) to Aug(1), which is detached from the positive D20 anomalies from the west (contour, Fig. 2b).

The evolution of the equatorial SST, surface wind and D20 anomalies during an ENSO event is quite well known and similar composites have been shown in Ren and Jin (2013). The evolutions of the SST and surface wind anomalies associated with El Niño and La Niña suggest that they are largely symmetric during their development and peak phases, and become largely asymmetric in the decay phase. Of particular interest to us is the rapid dissipation of the ENSO event from Jan(1) to Apr(1) after its maturing phase, which leads to the termination of an El Niño event and a significant weakening of a La Niña event. This is closely connected to the off-equatorial processes to be discussed in the next section.

4. Equatorial and off-equatorial connections

In this section we show that, during the ENSO evolution, the equatorial variations are closely connected to off-equatorial processes through zonal and meridional mass transports associated with the thermocline anomalies. We first describe the roles played by the meridional transport because of its close connections to the equatorial thermocline variations discussed in section 3. The zonal transport, however, plays a more important role in affecting the ENSO evolution in its maturing phase, which is discussed next.

a. Meridional transport

When the thermocline slope changes in the equatorial Pacific, the zonal thermocline gradient extends to off-equatorial oceans to generate geostrophic meridional currents there (Jin and An 1999). Together with the Ekman transport, this process causes substantial meridional mass transport divergence (convergence) anomalies in the central Pacific (150°E–150°W) for the El Niño (La Niña) (Clarke et al. 2007). Shadings in Fig. 2 show the composite evolution of the convergence of meridional transport anomalies smoothed by zonally running mean with a 20° longitude window along 5°N and 5°S during El Niño and La Niña. The positive (negative) values mean the water mass is pumped toward (away from) the equator across 5°N and 5°S. The meridional transport is superimposed upon the equatorial

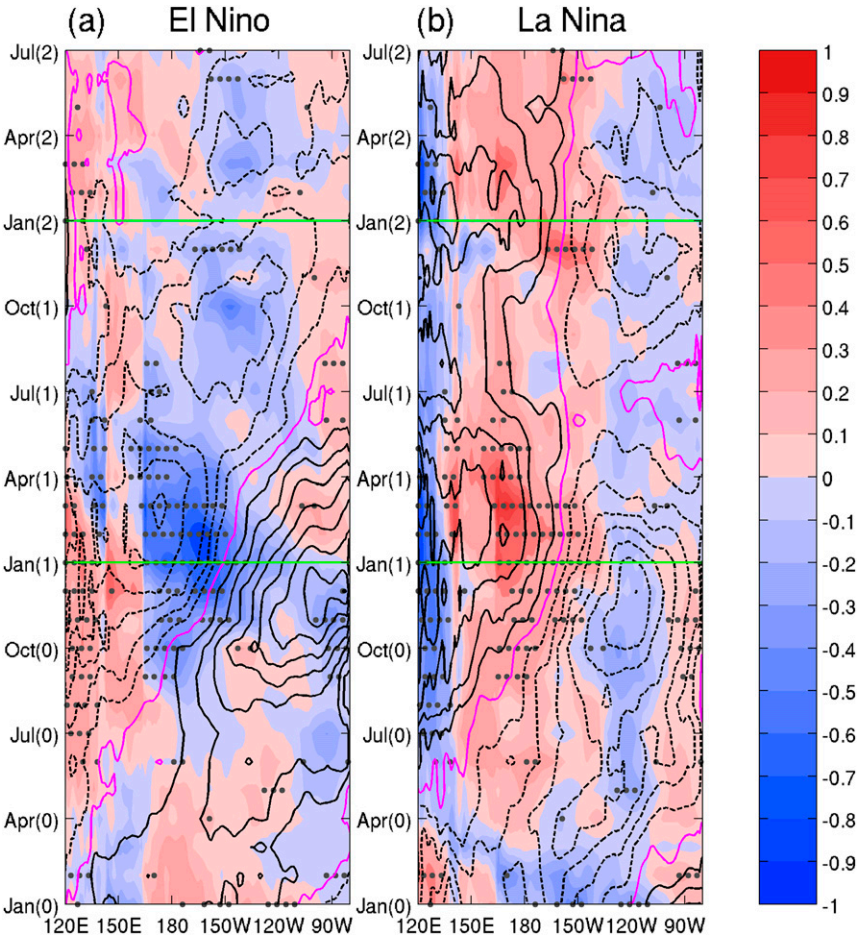

FIG. 2. Hovmöller diagram of D20 anomalies averaged between 5°S and 5°N (contour) and convergence of meridional transport anomalies smoothed by zonally running mean with 20° longitude window along 5°N and 5°S (shading) for the composite of (a) El Niño and (b) La Niña years. The positive (negative) value of shading means the water mass pump toward (away from) the equator across 5°N and 5°S. The purple lines represent zero D20 anomalies and solid (dashed) lines for positive (negative) D20 anomalies. The gray dots indicate the difference of transport between El Niño and La Niña exceeding a 95% confidence level using a *t* test. The contour interval is 5 m for D20 anomalies and shading interval is 0.1 Sv for transport anomalies ($1\ \text{Sv} \equiv 10^6\ \text{m}^3\ \text{s}^{-1}$). The green lines represent January of Year(1) and Year(2), respectively.

D20 anomalies to demonstrate their correspondence. The maxima of divergence and convergence (shading, Fig. 2) are usually collocated with the largest zonal gradient of D20 (contour, Fig. 2) while its general pattern is somewhat similar to the equatorial zonal wind anomalies (contour, Fig. 1), reflecting the effects by both geostrophic and Ekman flows (Clarke et al. 2007).

There are some interesting differences between the warm and cold events. For El Niño, the divergence (negative values of shading, Fig. 2a) starts from late summer of Year(0) and persisting well into the summer of Year(1). It also extends eastward from Aug(0) to Jan(1), following a similar migration of the anomalous westerlies (contour, Fig. 1a). For La Niña, however, the convergence (positive values of shading, Fig. 2b) starts somewhat earlier in Year(0) and persists longer, with its center always located in the western Pacific, which is also consistent with its corresponding wind structure (contour, Fig. 1b).

This meridional convergence–divergence corresponds to the recharge–discharge process described in previous studies (e.g., Jin 1997a,b). However, our result shows that, instead of a zonally uniform process, there is substantial zonal variation of meridional transport in ENSO. It is interesting to see that major discharge–recharge processes occur in the central and western Pacific. Chen et al. (2015) also indicate that the recharge–discharge process is reversed in the eastern

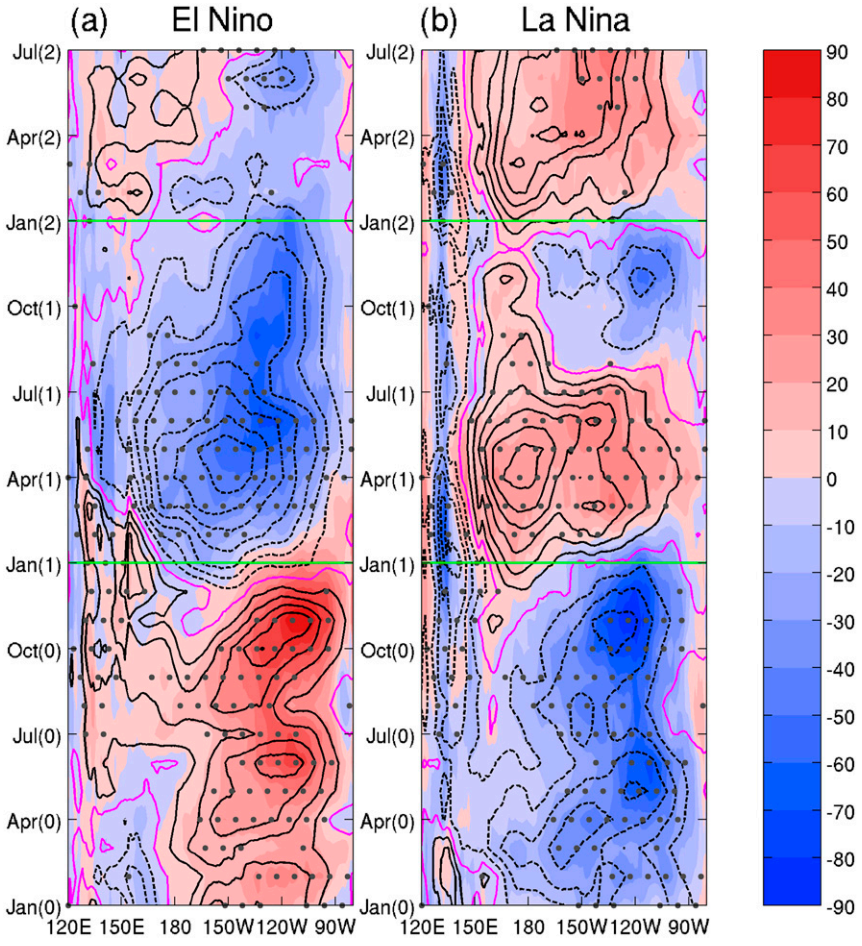

FIG. 3. Hovmöller diagram of E anomalies (shading) and zonal transport (contour) anomalies averaged between 5°S and 5°N for the composite of (a) El Niño and (b) La Niña years; E measures the relative magnitude of the $D20_{EQ}$ anomaly with respect to the off-equatorial ones ($D20_{5^\circ N}$ and $D20_{5^\circ N}$). The purple lines represent zero transport and solid (dashed) lines for positive (negative) transport anomalies. The gray dots indicate the difference of transport between El Niño and La Niña exceeding a 95% confidence level using a t test. The contour interval is 0.2 Sv for transport anomalies and shading interval is 10 m for E anomalies. The green lines represent January of Year(1) and Year(2), respectively.

Pacific. It seems that the major discharge–recharge processes are associated with the Sverdrup transports generated by the wind stress curls associated with the meridional gradient of the equatorial zonal wind stress anomalies. This relationship between the meridional convergence and the equatorial zonal wind stress can be seen in Figs. 1 and 2. Moreover, the different processes of meridional transport in the eastern and central-western regions also result from the opposite signs of their corresponding wind anomalies during the decaying phase for El Niño and during the developing phase to decaying phase for La Niña. The zonal variation of recharge–discharge process caused by zonal surface wind modifies the slope of thermocline, which may affect the efficiency of the Bjerknes feedback. This effect of meridional transport will be discussed in next subsection.

b. *Zonal transport*

As we will see in the next section, compared to the meridional transport, the zonal transport plays a more important role in the growth and termination of an ENSO event. The composite life cycles of the equatorial zonal transport for the El Niño and La Niña events are shown as the contours in Figs. 3a and 3b, respectively. The shading in Fig. 3 represents a quantity that further illustrates the mechanism to generate the equatorial zonal transport, which will be discussed in the later part of this section. During the developing phase of El Niño

(La Niña) [Year(0)], the eastward (westward) transport prevails in the central and eastern Pacific in two episodes, one from March to June, the other from August to November, with a break in July. These two episodes roughly correspond to the quick increase of the westerly (easterly) wind stress anomalies near or west of the date line (contour, Figs. 1a,b). These signals correspond to the zonal temperature advection described in Picaut et al. (1997), which enhances the thermocline feedback during the ENSO development, as suggested by An and Jin (2001).

The initial reversal of the zonal transport appears in Oct(0)–Nov(0) between 150°E and the date line where the signs of the equatorial D20 anomalies reversed a few months ago (contour, Fig. 2). At first, the reversed zonal transport propagates slowly eastward (contour, Fig. 3) with the eastward propagation of opposite D20 anomalies (contour, Fig. 2) from the western Pacific and reaches about 150°W by the end of the year. However, this corresponding relationship between zonal transport and equatorial D20 anomalies suddenly ends in Jan(1) when the reversed zonal propagations quickly extend eastward to occupy the whole basin (contour, Fig. 3). Between Jan(1) and Apr(1), the reversed zonal transports show a quick enhancement over the whole basin with its peak in the central Pacific around 150°W for the El Niño event in Apr(1). The peak in La Niña is in the same month but located farther to the west between 150°E and the date line although a secondary peak appears earlier in the central Pacific around 150°W. Therefore, at the peaking phase of both El Niño and La Niña, zonal transport quickly changes from enhancement to damping to the ENSO growth.

One should note that, among all equatorial variables we have examined, only the zonal transport shows the quick reversal at the peak phase of ENSO. Among the major factors of the Bjerknes feedback, the equatorial D20 anomalies initially associated with the reversed zonal transport propagate slowly in Year(1) at nearly the same pace as before and reach the eastern boundary in late spring and early summer (contour, Fig. 2). Similarly, the zonal wind stress anomalies are also largely sustained at a peak level between 150°W and 150°E before their demise in late spring of Year(1). It is also interesting to note that, after its peak, the relatively fast decay of the SST anomalies occurs in the eastern Pacific between 90° and 120°W (shading, Fig. 1), which can be readily explained as a direct response to the zonal transport reversal. On the other hand, the SST anomalies in the central Pacific (150°W to the date line), which are in balance with the zonal wind anomalies, are much more persistent after the peak of ENSO (Fig. 1). This longitudinal difference of the SST variation actually gives a perception of the westward propagation of the SST decaying signals. Moreover, the meridional transport (the discharge–recharge) also is largely maintained in the central and western Pacific without much change during the peak phase of ENSO (shading, Fig. 2). Overall, we argue that the reversal of the zonal transport contributes to damping ENSO.

Now we discuss the factors responsible for the zonal transport anomaly reversal. The geostrophic balance links the zonal velocity at the equator to the second derivative of D20 with respect to latitude as

$$\beta u_{\mathrm{EQ}} \approx -g' \frac{\partial^2 \mathrm{D20}}{\partial y^2}, \tag{1}$$

where $\beta = 2\Omega/R$, EQ is defined as 0°, and g' is the reduced gravity. In finite differencing format, $-(\partial^2 \mathrm{D20}/\partial y^2)$ is proportional to

$$\begin{aligned} E &= -[(\mathrm{D20}_{5^\circ\mathrm{N}} - \mathrm{D20}_{\mathrm{EQ}}) - (\mathrm{D20}_{\mathrm{EQ}} - \mathrm{D20}_{5^\circ\mathrm{S}})] \\ &= 2(\mathrm{D20}_{\mathrm{EQ}}) - \mathrm{D20}_{5^\circ\mathrm{N}} - \mathrm{D20}_{5^\circ\mathrm{S}}. \end{aligned} \tag{2}$$

In essence, E measures the relative magnitude of the $\mathrm{D20}_{\mathrm{EQ}}$ anomaly with respect to the off-equatorial ones ($\mathrm{D20}^{\circ}_{5\mathrm{N}}$ and $\mathrm{D20}^{\circ}_{5\mathrm{S}}$). Assuming that the D20 anomaly is symmetric to the equator, when E is positive, D20 concaves upward at the equator and the geostrophic zonal transport is eastward. Similarly, when E is negative, or D20 anomaly concaves downward at the equator, the geostrophic zonal transport anomaly is westward.

The Hovmöller diagram of E is shown in Fig. 3 as shadings. Clearly, E corresponds well with the zonal transport anomaly above D20 throughout the life cycle of both El Niño and La Niña, confirming that the equatorial zonal transport anomaly is predominantly geostrophic (Jin and An 1999). More interestingly, both the gradual reversal of the zonal transport anomaly first initiated in the western Pacific in Oct(0)–Nov(0) and the sudden basinwide reversal around Jan(1) are associated with the sign changes of E. Since E is determined by both the $\mathrm{D20}_{\mathrm{EQ}}$ and off-equatorial D20 anomalies, we can identify the zonal transport anomaly as mainly driven by the former or the latter in different phases of the ENSO evolution. During Oct(0)–Nov(0), the initial reversal of the zonal transport anomaly is apparently driven by $\mathrm{D20}_{\mathrm{EQ}}$ anomaly as shown by its close correspondence with the local D20 anomalies on the equator (contour, Fig. 2). It is not surprising that, for an El Niño event, the westward transport anomaly first appears in the longitude band of 150°E to the date line where the westerly wind stress (contour, Fig. 1a) and meridional divergence anomalies are largest (shading, Fig. 2a).

As a result, the strong discharge process causes substantial shoaling of the thermocline, making the $D20_{EQ}$ anomaly shallower than the off-equatorial ones. A similar situation occurs in the same phase of the La Niña event in opposite sign to the El Niño event. Although the controlling factor of the zonal transport is taken over by another mechanism, as we describe below, we expect that the $D20_{EQ}$ mechanism will continue a relatively slow paced eastward propagation in the El Niño case while stay more or less stationary in the La Niña case, as manifested by their corresponding D20 evolution on the equator (contour, Fig. 2).

On the other hand, the basinwide reversal of the equatorial zonal transport anomaly in Jan(1) is mainly induced by the off-equatorial D20 anomaly that extends westward from the eastern boundary near 5°N and 5°S. The eastward propagating D20 anomalies along the equator reach the oceanic eastern boundary in boreal winter at the peak phase of ENSO (contour, Fig. 2). Subsequently, the D20 anomalies in the eastern boundary are reflected as Rossby waves and propagate westward off the equators on both hemispheres toward the central Pacific. As a result, E changes sign, and so does the zonal transport anomaly. The branching off of the D20 anomaly near the equator in Jan(1) can be seen clearly from the zonally averaged D20 anomaly between 80°W and the date line in Figs. 4 and 5 (shading). In the El Niño event (Fig. 4), the D20 anomaly at the equator switches from maximum to minimum and the meridional gradient of D20 is reversed in both hemisphere in Jan(1) (contour, Fig. 4a). A similar reversal also occurs in La Niña (Fig. 5) during Jan(1). In both cases, the poleward propagation of the D20 anomalies from the equator to about 10°N and 10°S from Jan(1) to May(1) lead to the opposite gradient of D20 anomaly after the peak of ENSO (Figs. 4a and 5a). As the result, the equatorial zonal transport anomaly is reversed and extends to off-equator (contour, Figs. 4b and 5b) after Jan(1), which is strongest during Mar(1) and Apr(1). It should be pointed out that the total zonal transport anomaly is the combination of both factors caused by $D20_{EQ}$ mechanism and off-equatorial D20 mechanism.

To further demonstrate the evolution of D20 and zonal transport anomalies, Figs. 6 and 7 show the composites of the zonal transport (contour) and D20 (shading) anomalies for El Niño and La Niña years from Sep(0) to Aug(1), respectively. According to these composites, the D20 anomalies propagate eastward along the equator [Sep(0) to Nov(0)] and reach the east boundary in Dec(0). Meanwhile, the reversed zonal transport anomaly appears around the date line in Sep(0) and extends eastward to about 150°W by Dec(0). The reversed zonal transport anomaly is limited in 2°S–2°N and, as we discussed above, is driven by local zonal wind stress associated with ENSO. After the peak of ENSO, the D20 anomalies are reflected in the eastern Pacific and then propagate westward off the equator. As discussed in Hu et al. (2014), these reflected D20 anomalies make the D20 anomalies in the off-equator areas higher than at the equator for El Niño events and lower for La Niño events after Dec(0). The meridional structure of the thermocline rapidly generates reversed zonal transport in the eastern equatorial Pacific, which is combined with the existing ones farther to the west and forms the reversed zonal transport anomaly in the whole Pacific basin in 5°S–5°N. The reversed zonal transport anomaly after the mature phase quickly weakens the ENSO-associated SST anomalies in the eastern Pacific.

c. *Equatorial mass and heat budget*

Many previous studies have emphasized the role of SST advection of the equatorial zonal current anomalies during an ENSO event (e.g., Picaut et al. 1997; An and Jin 2001). Through this process, the anomalous zonal current modifies the equatorial SST anomalies. On the other hand, anomalous zonal transport anomaly also redistributes water above the thermocline along the equatorial ocean and directly affects the zonal tilting of the thermocline depth, a critical factor of ENSO growth. This process can be considered as an ''oceanic'' factor because it does not change SST or surface winds directly. In this subsection, we examine how effective this oceanic contribution is and whether it can be considered as an independent factor in ENSO evolution.

The meridional transport anomaly (i.e., recharge–discharge processes) changes WWV in the equatorial Pacific. In addition to influencing the mass balance, it is responsible for the ocean heat exchange processes between the equatorial and the off-equatorial oceans that cause the ENSO phase transition (Jin 1997a,b; Meinen and McPhaden, 2000; Kumar and Hu 2014). Here we define an anomalous WWV index as the integrated volume of water above D20 within 5°S–5°N from 120°E to 80°W (Meinen and McPhaden, 2000; Kumar and Hu 2014). In both El Niño and La Niña events, the tendency of the WWV index (gray bars, Figs. 8b,c) is primarily contributed by the net meridional transport anomaly (blue curves, Figs. 8b,c). The magnitude of the net zonal transport anomaly (red curves, Figs. 8b,c) is much smaller than that of meridional transport anomaly and is negligible when the whole Pacific basin is considered. The zonal surface wind anomalies (dashed curves, Fig. 8a) lead Niño-3.4 index (solid curves, Fig. 8a) by about 1–3 months. We also find that the Niño-3.4 index is out of phase with the WWV tendency.

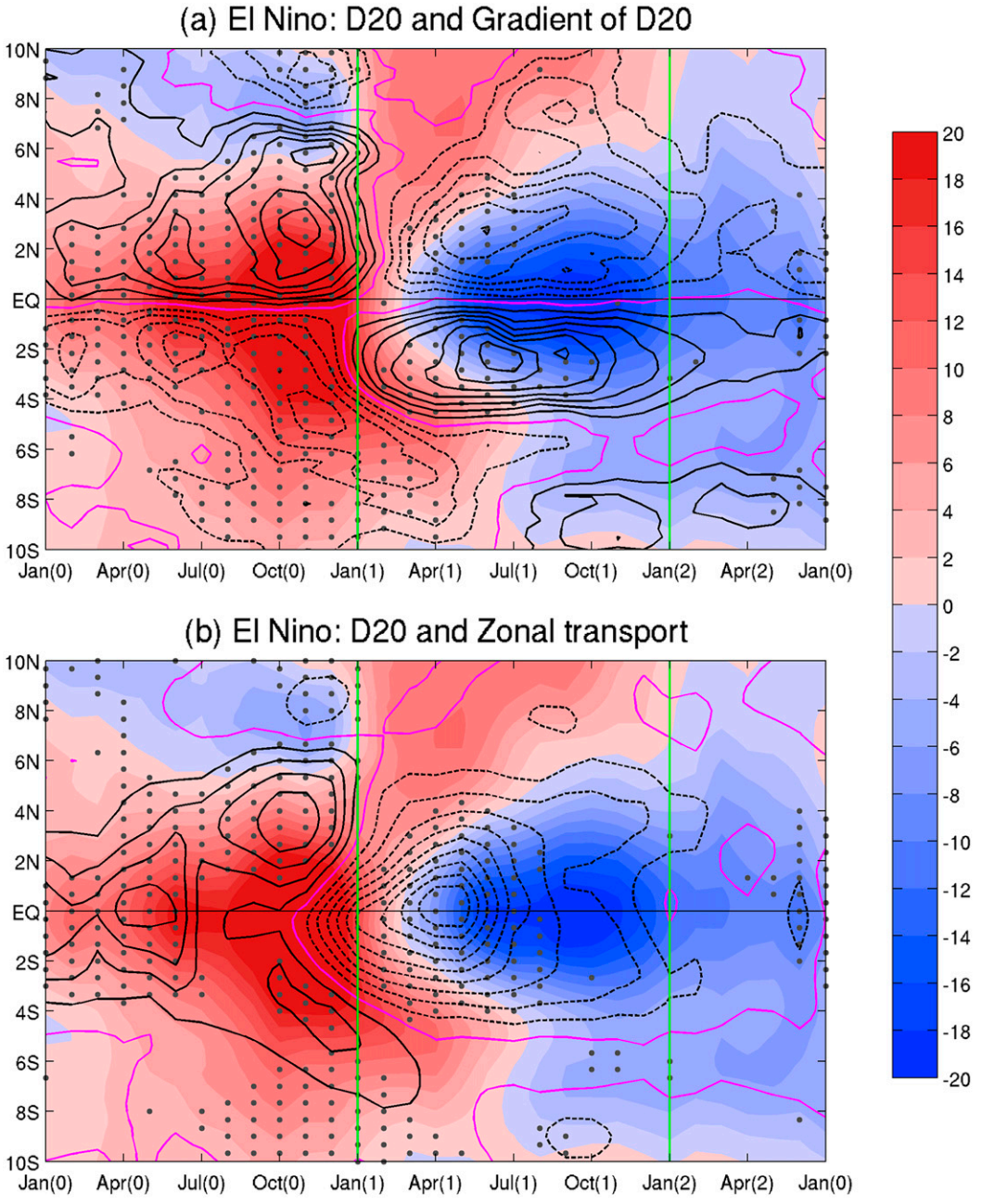

FIG. 4. Time–latitude evolutions for composites of El Niño years. The shading represents the D20 anomalies averaged in 180°–80°W in all panels. The contours represent meridional gradient of D20 anomalies in (a) and zonal transport anomalies in (b). The purple lines represent zero anomalies and solid (dashed) lines for positive (negative) transport anomalies. The gray dots in (a) and (b) respectively indicate the difference of gradient of D20 and transport between El Niño and La Niña exceeding a 95% confidence level using a *t* test. The shading interval is 2 m for D20 anomalies and contour interval is 1 meter per degree for gradient of D20 anomalies in (a) and 0.2 Sv for transport anomalies in (b). The green lines represent January of Year(1) and Year(2), respectively.

The zonal transport anomaly, however, not only redistributes mass along the equator but also changes the heat balance above the thermocline in the eastern equatorial Pacific. In particular, this process works directly against the zonal tilting of equatorial thermocline. We choose 160°W, the midpoint between the positive and negative D20 anomalies (contour, Fig. 2), as a check point in Fig. 9 to discuss the thermocline heat budget in the eastern equatorial Pacific (5°S–5°N, 160°–80°W) contributed from zonal, meridional, and vertical heat

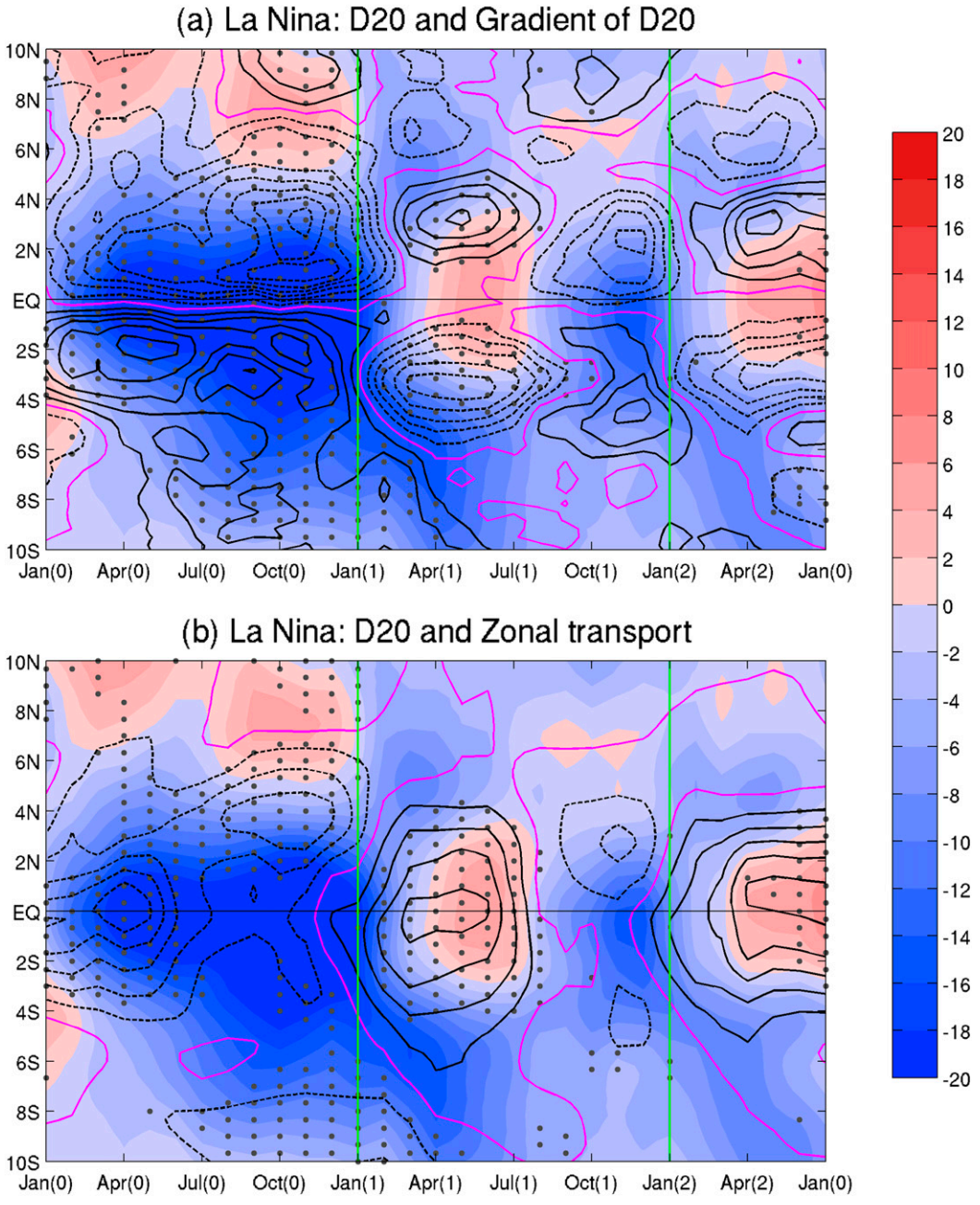

FIG. 5. As in Fig. 4, but for La Niña years.

transport. Here we analyze the thermocline heat budget instead of the mixed-layer heat budget because of the equatorial transport above the thermocline, which is predominantly geostrophic; however, the mixed-layer transport is partly dominated by the Ekman transport. The thermocline heat budget equation is

$$\frac{\partial \mathrm{HC}}{\partial t} = Q_u + Q_v + Q_w + Q_q + R, \qquad (3)$$

where the term in the left side represents the tendency of heat content above the thermocline; Q_u, Q_v, and Q_w denote the zonal, meridional, and vertical heat convergence, respectively; Q_q indicates the total downward heat at surface; and R is the residual term. Here we define an anomalous heat content above the thermocline as the integrated heat content of water above D20 within 5°S–5°N from 160° to 80°W. The time tendency of the anomalous heat content integrated within this

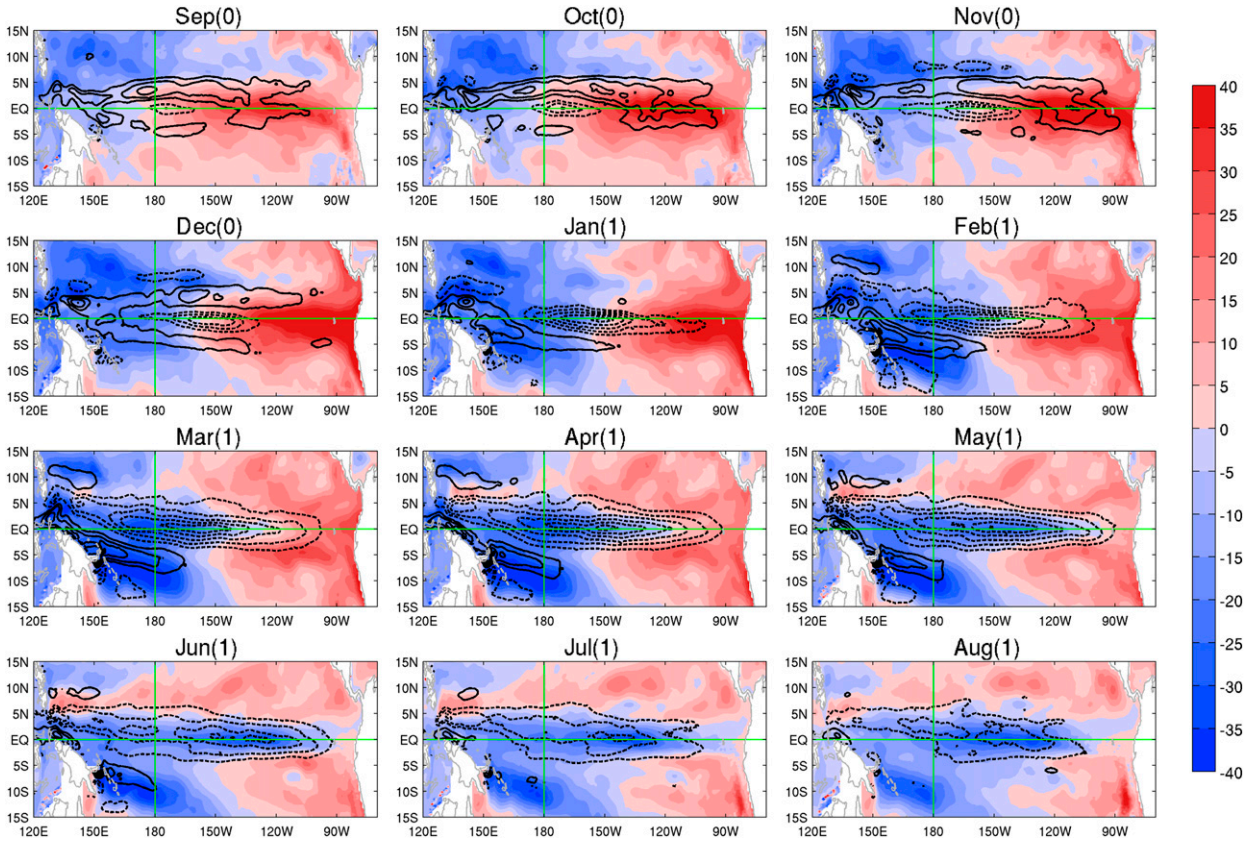

FIG. 6. Composites of the zonal transport (contour) and D20 (shading) anomalies for El Niño years. The interval is 5 m for D20 anomalies, and 0.5 Sv for zonal transport anomalies (solid curves are positive and dashed curves are negative).

volume is contributed by the zonal and meridional heat convergence, defined as the net heat transport into the eastern equatorial Pacific across the horizontal boundaries. The vertical heat transport is contributed by the net heat transport into the eastern equatorial Pacific across the surface of D20. The total downward surface heat is estimated as the integrated downward heat flux in the eastern equatorial Pacific at surface. It is worth noting that the surface heat term is two orders of magnitude smaller than other terms when we consider the thermocline heat budget integrated from surface to depth of D20. These terms are estimated explicitly using the GODAS monthly mean analysis. The residuals include the horizontal and vertical diffusions and the contributions of the unresolved higher-frequency eddy transports. The tendency of the heat content (gray bar, Figs. 9b,c) corresponds well with the tendency of SST anomalies in the eastern equatorial Pacific (solid curves, Fig. 9a). This result indicates that the eastern Pacific SST anomaly is strongly driven by local heat content variation. During the developing phase, the zonal heat transport anomaly (red curves, Figs. 9b,c) enhances the thermocline feedback in both El Niño and La Niña events. The reversal of the zonal transport anomaly appears in Oct(0)–Nov(0), which is nearly simultaneous with the time when the heat content anomaly in the eastern Pacific starts to decay. The weakening of the surface wind anomalies (dashed curves, Fig. 9a), which occurred in response to the weakening of the SST anomalies in the eastern equatorial Pacific, may also change the zonal thermocline slope through the readjustment of the Sverdrup balance, resulting in a change of the thermocline depth in the eastern equatorial Pacific. However, the direct influence on thermocline anomaly in the eastern Pacific associated with reversed zonal transport anomaly is independent of that of the equatorial zonal wind stress anomalies.

The net meridional heat transport anomaly may also be able to contribute to the thermocline feedback because of its substantial zonal variation as we have shown in Fig. 2 (shading). However, the contribution from the meridional heat transport anomaly is smaller than that from the zonal heat transport anomaly in the eastern Pacific (cf. the curves in Figs. 9b,c). During the developing phase in El Niño events, the major recharge processes occur in the central Pacific and few discharge

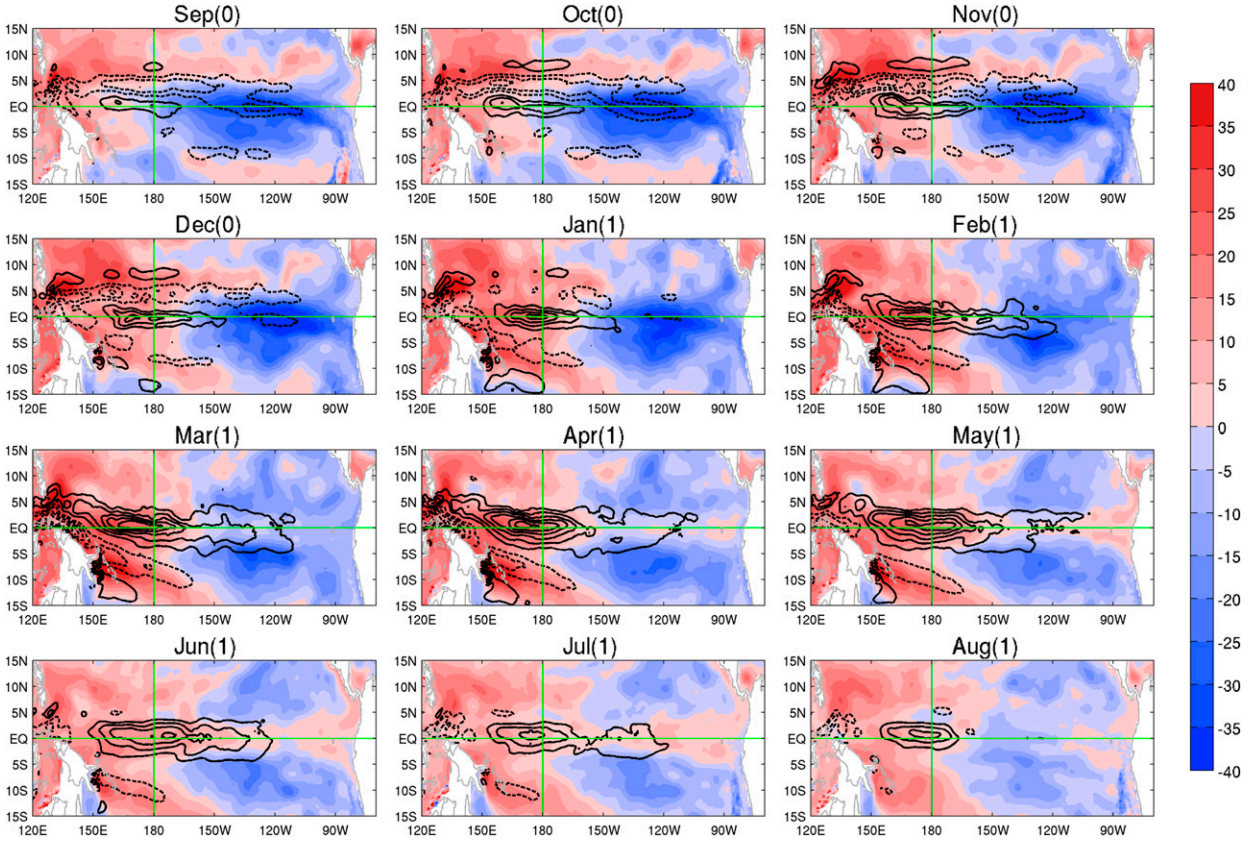

FIG. 7. As in Fig. 6, but for La Niña years.

processes in the eastern Pacific. As a result, the meridional heat transport in the eastern Pacific (blue curves, Fig. 9b) reduces the heat content in the eastern equatorial Pacific. The water heat of the eastern Pacific keeps being lost due to the largest meridional divergence. For La Niña, however, the convergence starts somewhat from late winter in Year(0) and persists longer, with its center always located in the western Pacific (shading, Fig. 2). Consequently, the value of meridional heat transport anomaly (blue curves, Fig. 9c) is zero in the eastern Pacific. However, the recharge processes extend eastward at the peak of La Niña in Jan(1) and Dec(1) and this extension of convergence of meridional heat transport anomaly will increase the heat content in the eastern Pacific and reduce the effect of building zonal tilting. Although the meridional heat transport anomaly would changes the heat budget as the ENSO events mature, the zonal heat transport plays the leading role in causing the decrease of the upper ocean heat content in the eastern equatorial Pacific Ocean after the ENSO peaking phase.

The vertical heat transport anomaly is a damping term for the thermocline heat budget in the eastern Pacific (black curves, Figs. 9b,c). Because the vertical heat transport is defined as the net transport of the 20°C water across the surface of D20, the contribution of vertical heat transport is mainly determined by the vertical velocity in this calculation. This contribution, however, is always partly offset by a corresponding displacement of the D20 surface itself. The effect of the latter part is not explicitly evaluated and is contained in the residual term R. The vertical heat transport is out of phase with zonal heat transport anomaly and the vertical transport along the equator is dynamically associated with zonal transport (Su et al. 2010). The relationship between zonal and vertical heat transport anomaly can be explained by the mass conservation. To further demonstrate the evolution of thermocline and the relationship between zonal and vertical transport anomalies, Figs. 10 and 11 show the evolution of the zonal velocity anomalies (contour) and vertical velocity anomalies (shading) in connection with the fluctuation of the thermocline (D20; red curves) for El Niño and La Niña years from Jun(0) to May(1), respectively, together with climatological D20 (green curves). During the developing phase of El Niño (La Niña) [Jul(0)–Aug(0)], the eastward (westward) velocity prevails above D20 and enhances the thermocline feedback during the ENSO development. At the same time, the major

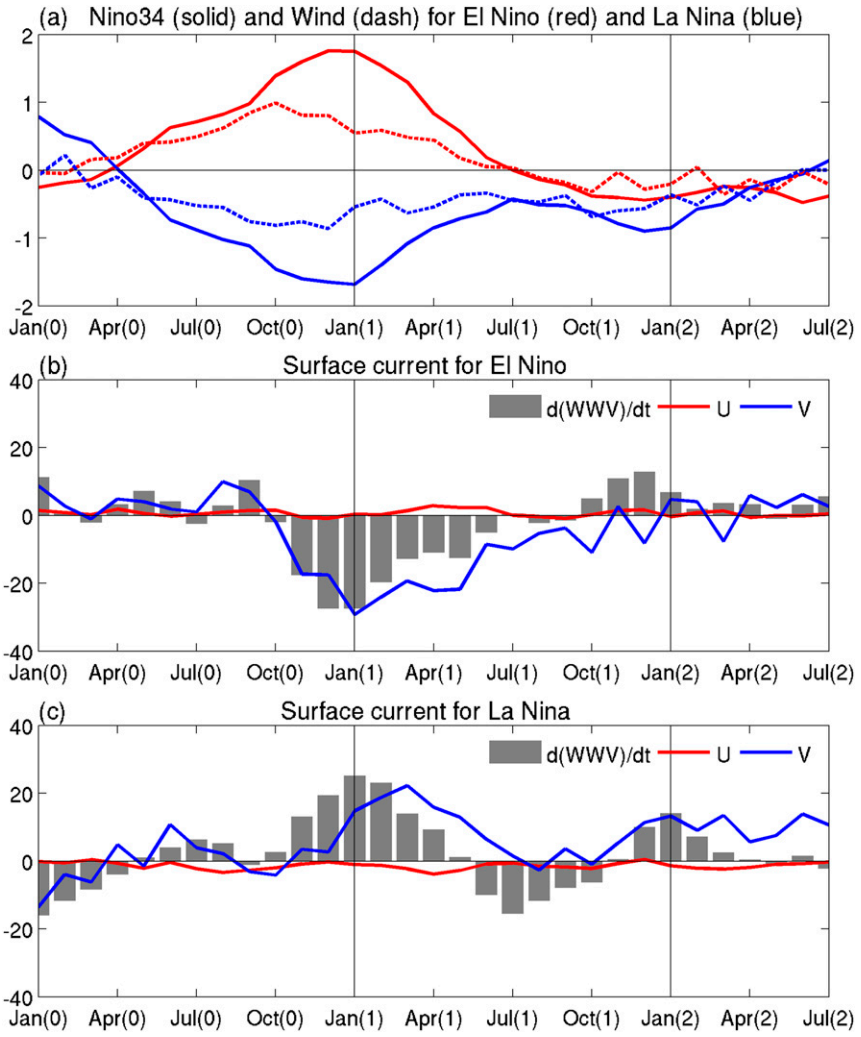

FIG. 8. In (a), the solid curves are the SST anomalies averaged over the Niño-3.4 region (5°S–5°N, 120°–170°W) and dashed curves are the zonal surface wind anomalies averaged between 5°S and 5°N, extending longitudinally from 120°E to 80°W for El Niño (red curves) and La Niña (blue curves) years. The gray bar is the tendency of the WWV index averaged between 5°S and 5°N, extending longitudinally from 120°E to 80°W. The red curves represent the zonal transport convergence anomalies integrated from 5°S to 5°N along 120°E and 80°W and the blue curves represent the meridional transport convergence anomalies integrated from 120°E to 80°W along 5°S and 5°N for El Niño (b) and La Niña (c) years. (Units are °C for SST anomalies, m s^{-1} for surface wind and Sv for transport and tendency of WWV.)

downward (upward) velocity generated by the eastward (westward) velocity occurs in the eastern Pacific (100°–80°W) to slow down the development of El Niño (La Niña). The first reversed zonal velocity anomaly appears along D20 around the date line in Sep(0) and extends eastward to about 150°W by Dec(0), as we have shown in Figs. 6 and 7. However, the eastward (westward) velocity anomaly still prevails in the upper layer above 100 m. The upward (downward) velocity anomaly appears along the east edge of reversed zonal velocity anomaly and propagates eastward with it. Between Jan(1) and May(1), the reversed zonal velocity anomaly shows a quick enhancement over the whole layer above D20. The reversed zonal velocity anomaly after the mature phase quickly weakens the thermocline feedback associated with SST anomalies in the eastern Pacific. Nevertheless, the upward (downward) velocity anomaly locates in the far eastern Pacific along the east edge of the reversed zonal velocity to work against the decay of El Niño (La Niña). This result demonstrates the close connection of the zonal and vertical transport anomalies, with the reversal of the zonal transport above

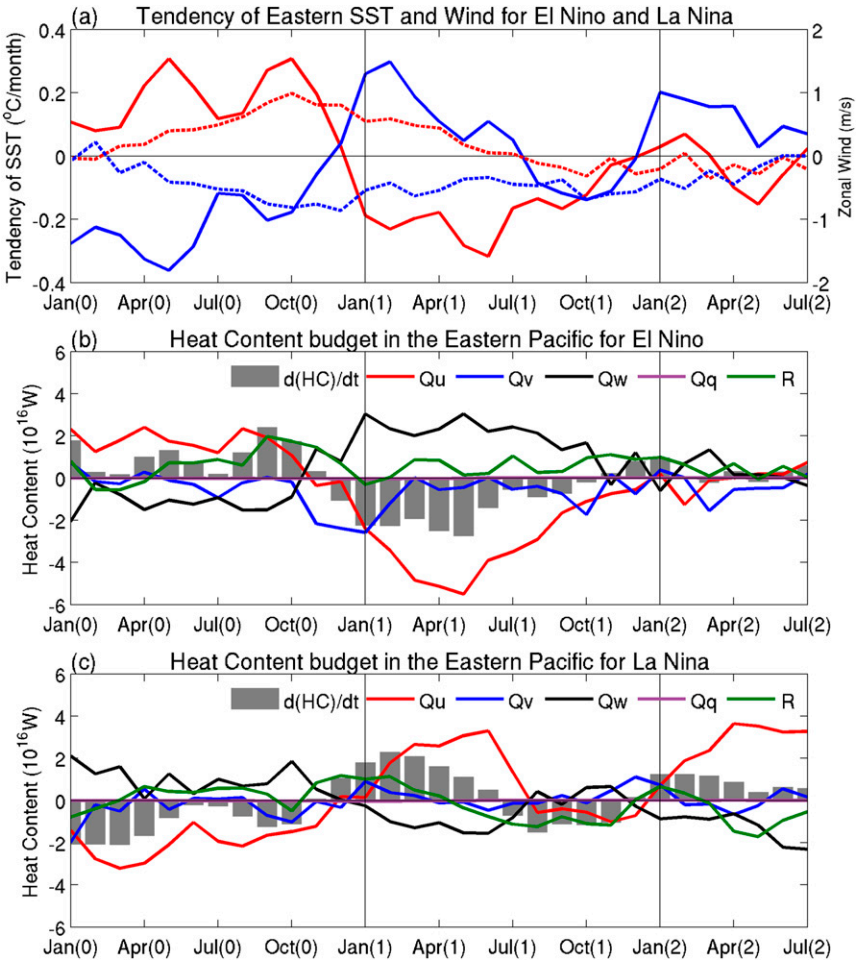

FIG. 9. (a) Solid curves are the tendency of SST anomalies averaged in the eastern Pacific region (5°S–5°N, 160°–80°W) and dashed curves are the zonal surface wind anomalies averaged between 5°S and 5°N, extending longitudinally from 120°E to 80°W for El Niño (red curves) and La Niña (blue curves) years. Also shown are the time evolutions of thermocline heat budget in eastern Pacific (5°S–5°N, 160°W–80°W) for composites of (b) El Niño and (c) La Niña years. The gray bar is the tendency of heat content above D20 in the eastern Pacific. The red, blue, and black curves represent the zonal, meridional, and vertical heat transport, respectively. The purple curves represent the total downward heat at surface. The green curves show the residual term. (Units are °C month^{-1} for tendency of SST anomalies, m s^{-1} for surface wind, and W for heat budget.)

the thermocline in the El Niño (La Niña) mature phase corresponding to the switch from downwelling (upwelling) to upwelling (downwelling) in the eastern Pacific. Since the reversal of the zonal transport is mainly associated with the reflected off-equatorial thermocline anomalies, we argue that, at this moment, it is the zonal transport drives the vertical transport change, instead of the other way around.

5. Summary and discussion

In this work, a sudden reversal of the zonal equatorial upper current at the peaking phase of ENSO is revealed to explain the rapid termination of an ENSO event. This process is dependent upon the fact that the equatorial zonal current is mainly controlled by the relative strengths of the thermocline depth anomalies on and off the equator (i.e., the concavity of the thermocline meridional structure), through geostrophic balance.

During the developing phase of ENSO, the zonal surface wind anomalies show a physically consistent pattern with the corresponding SST anomalies. The peak of wind anomaly is collocated with minimum or maximum zonal gradients of SST anomalies. The zonal gradient of the equatorial thermocline anomalies is proportional to the surface wind and thus to the SST anomaly. The wind-driven thermocline anomalies in the eastern Pacific

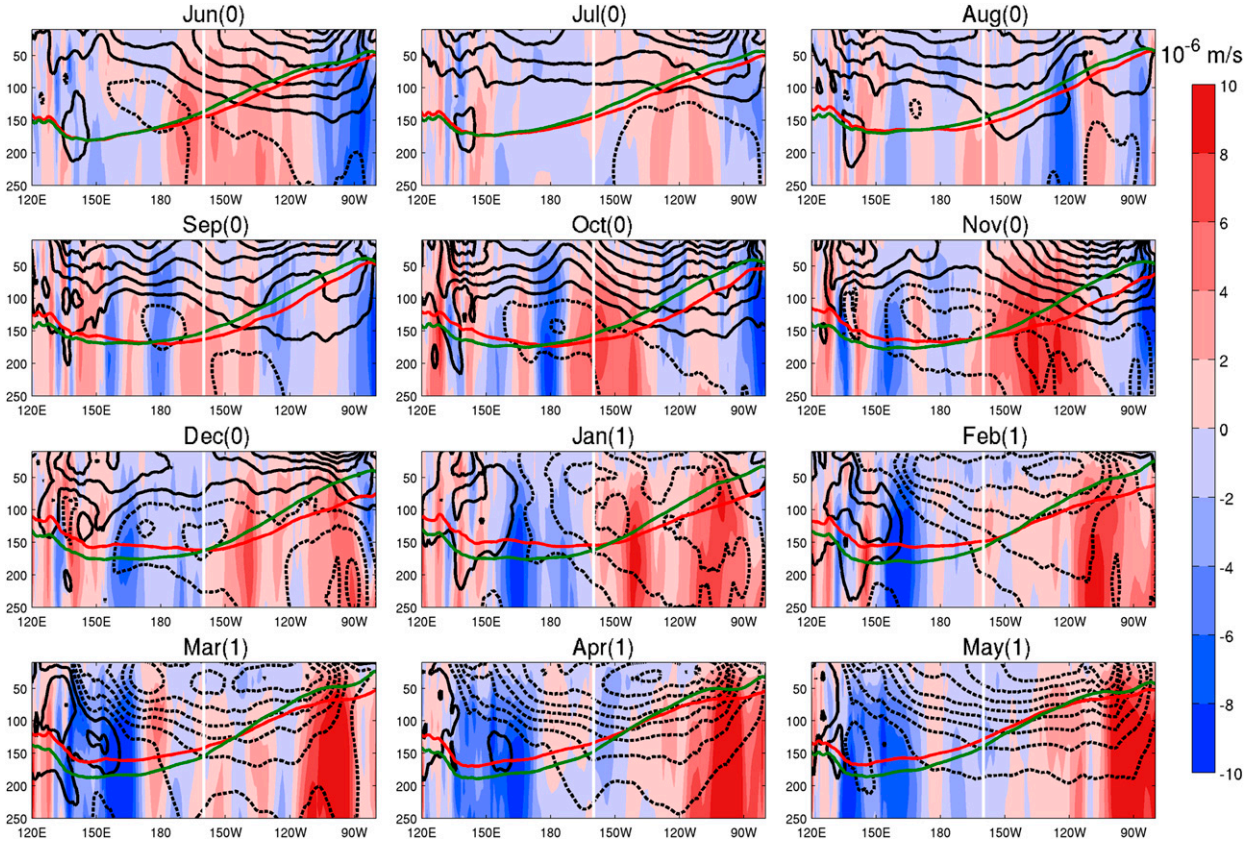

FIG. 10. Composites of the zonal velocity (contour) and vertical velocity (shading) anomalies averaged between 5°S and 5°N for El Niño years. The red (green) curve represents the D20 (climatology of D20). The white line represents the 160°W (climatology of D20). The interval is 2×10^{-6} m s^{-1} for vertical velocity anomalies, and 1 m s^{-1} for zonal velocity anomalies (solid curves are positive and dashed curves are negative).

manifest the subsurface component of the positive ocean–atmosphere feedback process that brings El Niño or La Niña to a mature phase. The ENSO is amplified through this coupled process between ocean and atmospheric anomalies in the central and eastern equatorial Pacific. Furthermore, the equatorial thermocline anomalies are largest and determine the zonal transport anomalies. Since the zonal wind anomalies over the western-central equatorial ocean generate opposite equatorial thermocline anomalies locally and farther to the east, opposite zonal transport anomalies form in the western-central and central-eastern equatorial Pacific, respectively. At this stage, the anomalous zonal transport in the east enhances the ENSO growth through zonal SST advection.

In the mature phase of ENSO, off-equatorial thermocline depth anomalies become more dominant in the eastern Pacific due to the reflection equatorial signals at the eastern boundary and their westward propagation in both hemispheres. As a result, the concavity of the thermocline anomalies at the equator is reversed in the east (i.e., the off-equatorial thermocline depth anomalies become higher than that on the equator for El Niño events and lower for La Niño events). This change of the meridional thermocline structure reverses zonal transport rapidly in the central-to-eastern equatorial Pacific, which is joined with the existing zonal transport anomalies farther to the west and forms a basinwide current reversal throughout the equatorial Pacific. This basinwide transport reversal weakens the ENSO SST anomalies through advection damping. More importantly, the reversed zonal mass transport anomaly reduces the existing zonal tilting of equatorial thermocline and suppresses its feedback to wind anomalies effectively. We argue that reversal of the equatorial zonal transport is a critical factor in terminating an ENSO event. Although there are other factors that also contribute to the termination of ENSO events, the basinwide current reversal mechanism associated with reflective thermocline depth anomalies is a robust ocean dynamic process that is built in to the peak phase of ENSO as a dynamic feedback within the ocean that has functions in both El Niño and La Niña.

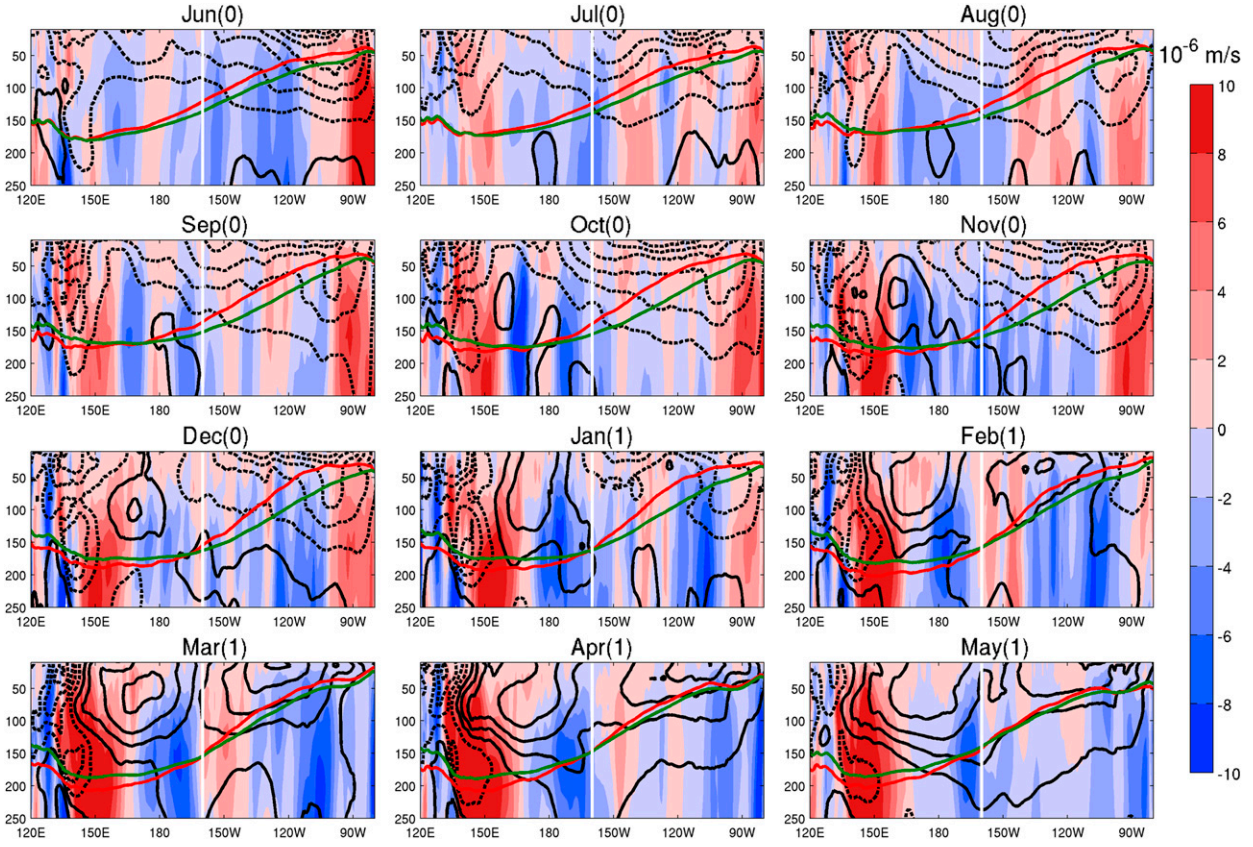

FIG. 11. As in Fig. 10, but for La Niña years.

The meridional transport anomaly is connected with ENSO phase transition by exchanging the ocean heat between the equatorial and off-equatorial ocean. In addition to Ekman transport, a substantial portion of the meridional transport anomaly is generated by the zonal thermocline gradient anomaly according to geostrophic balance. Consequently, the maxima of divergence and convergence anomalies are collocated to the largest zonal gradient of thermocline while their general pattern is somewhat similar to the equatorial zonal wind stress anomalies. Although the zonally integrated meridional transport anomaly largely fulfills the role of recharge–discharge to the upper ocean warm water volume, there is substantial zonal variation of meridional transport anomaly due to the pattern of zonal surface wind anomaly, which redistributes the slope of the thermocline and may affect the efficiency of Bjerknes feedback.

The vertical heat transport anomaly is a damping term in an ENSO event. The vertical transport is out of phase with zonal transport anomaly and the vertical transport along the equator is dynamically associated with zonal transport. The relationship between zonal and vertical transport anomalies can be explained by the mass conservation. Our results demonstrate the close connection of the zonal and vertical transport anomalies, with the reversal of the zonal transport above the thermocline in the El Niño (La Niña) mature phase corresponding to the switch from downwelling (upwelling) to upwelling (downwelling) in the eastern Pacific.

In this paper, we emphasize the reversal of the zonal equatorial transport anomaly as an ENSO termination mechanism that is functional for both El Niño and La Niña events. However, an interesting asymmetry also appears between the warm and cold events. During the development phase, the anomaly patterns are quite symmetric between El Niño and La Niña events. The processes of ENSO weakening by the reversed zonal transport after the mature phase are also symmetric between El Niño and La Niña years. However, the asymmetric features appear after their peak. For instance, the negative SST and westerly surface wind anomalies, for an El Niño year, start to propagate eastward in May(1) and reach the central Pacific in the summer of Year(1) and turn into cold phase after the mature phase. For La Niña, however, the positive SST and easterly surface wind anomalies remain stationary in the western equatorial Pacific throughout Year(0) to Year(1) without any propagation. The asymmetry

in the temporal evolution between El Niño and La Niña has been attributed to a couple of reasons. One explanation is that the interannual variation of tropical instability waves slows down the transition from La Niña to El Niño but does not have a significant impact on the transition from El Niño to La Niña (Nagura et al. 2008). Another possible explanation is the nonlinear atmospheric response to the SST distribution in the equatorial Pacific and the surrounding tropical Pacific and Indian Ocean such that surface wind forcing in the far western equatorial Pacific tends to efficiently terminate the warm phase into the La Niña condition (Weisberg and Wang 1997; Wang et al. 1999) but to prolong the cold phase before the El Niño condition (Hoerling et al. 1997; Kug and Kang 2006; Ohba and Ueda 2009; Okumura and Deser 2010; Okumura et al. 2011; Ohba and Watanabe 2012). Hu et al. (2014) argued that the persistence of the cold condition is related to the equatorial upwelling Kelvin waves and the reflected off-equatorial Rossby wave in stronger La Niña events. Another explanation provided by Chen et al. (2016) shows that the dynamic processes associated with asymmetry of wind response in the western Pacific is as important as the thermodynamic processes related to the asymmetric cloud–radiation–SST and evaporation–SST processes in contributing to the ENSO evolution asymmetry. The reversed zonal transport also appears to be asymmetric between El Niño and La Niña in this study. The peak of reversed zonal transport in El Niño locates between 120°W and the date line; however, the reversed transport in La Niña locates farther to the west between 150°E and the date line (Fig. 3). This difference of spatial pattern between warm and cold event leads to the fact that the amplitude of the reversed zonal transports anomalies associated with tilting along 160°W in El Niño is larger than that in La Niña (Fig. 9). The reversed zonal transport anomaly after the mature phase weakens El Niño in the eastern Pacific more efficiently than for La Niña.

Acknowledgments. This work is supported by the Ministry of Science and Technology (104-2917-I-002-012 and 104-2111-M-002-001). The authors thank all colleagues and students who contributed to this study. Bohua Huang is supported by grants from NSF (AGS-1338427), NOAA (NA14OAR4310160), and NASA (NNX14AM19G).

REFERENCES

An, S. I., and F.-F. Jin, 2001: Collective role of thermocline and zonal advective feedbacks in the ENSO mode. *J. Climate*, **14**, 3421–3432, doi:10.1175/1520-0442(2001)014<3421:CROTAZ>2.0.CO;2.

Battisti, D. S., and A. C. Hirst, 1989: Interannual variability in a tropical atmosphere–ocean model: Influence of the basic state, ocean geometry and nonlinearity. *J. Atmos. Sci.*, **46**, 1687–1712, doi:10.1175/1520-0469(1989)046<1687:IVIATA>2.0.CO;2.

Behringer, D. W., and Y. Xue, 2004: Evaluation of the global ocean data assimilation system at NCEP: The Pacific Ocean. *Eighth Symp. on Integrated Observing and Assimilation Systems for Atmosphere, Oceans, and Land Surface*, Seattle, WA, Amer. Meteor. Soc., 2.3. [Available online at https://ams.confex.com/ams/pdfpapers/70720.pdf.]

Bjerknes, J., 1969: Atmospheric teleconnections from equatorial Pacific. *Mon. Wea. Rev.*, **97**, 163–172, doi:10.1175/1520-0493(1969)097<0163:ATFTEP>2.3.CO;2.

Boulanger, J.-P., and C. Menkes, 1999: Long equatorial wave reflection in the Pacific Ocean from TOPEX/POSEIDON data during the 1992–1998 period. *Climate Dyn.*, **15**, 205–225, doi:10.1007/s003820050277.

——, and ——, 2001: The Trident Pacific model. Part 2: Role of long equatorial wave reflection on sea surface temperature anomalies during the 1993–1998 TOPEX/POSEIDON period. *Climate Dyn.*, **17**, 175–186, doi:10.1007/PL00013734.

——, S. Cravatte, and C. Menkes, 2003: Reflected and locally wind-forced interannual equatorial Kelvin waves in the western Pacific Ocean. *J. Geophys. Res. Oceans*, **108**, 3311, doi:10.1029/2002JC001760.

Cai, M., 2003: Formation of the cold tongue and ENSO in the equatorial Pacific basin. *J. Climate*, **16**, 144–155, doi:10.1175/1520-0442(2003)016<0144:FOTCTA>2.0.CO;2.

Chen, H.-C., C. H. Sui, Y. H. Tseng, and B. H. Huang, 2015: An analysis of the linkage of Pacific subtropical cells with the recharge–discharge processes in ENSO evolution. *J. Climate*, **28**, 3786–3805, doi:10.1175/JCLI-D-14-00134.1.

Chen, M., T. Li, X. Shen, and B. Wu, 2016: Relative roles of dynamic and thermodynamic processes in causing evolution asymmetry between El Niño and La Niña. *J. Climate*, **29**, 2201–2220, doi:10.1175/JCLI-D-15-0547.1.

Clarke, A. J., S. V. Gorder, and G. Colantuono, 2007: Wind stress curl and ENSO discharge/recharge in the equatorial Pacific. *J. Phys. Oceanogr.*, **37**, 1077–1091, doi:10.1175/JPO3035.1.

Harrison, D. E., 1987: Monthly mean island surface winds in the central tropical Pacific and El Niño events. *Mon. Wea. Rev.*, **115**, 3133–3145, doi:10.1175/1520-0493(1987)115<3133:MMISWI>2.0.CO;2.

——, and N. K. Larkin, 1998: El Niño–Southern Oscillation sea surface temperature and wind anomalies, 1946–1993. *Rev. Geophys.*, **36**, 353–399, doi:10.1029/98RG00715.

——, and G. A. Vecchi, 1999: On the termination of El Niño. *Geophys. Res. Lett.*, **26**, 1593–1596, doi:10.1029/1999GL900316.

Hoerling, M. P., A. Kumar, and M. Zhong, 1997: El Niño, La Niña, and the nonlinearity of their teleconnections. *J. Climate*, **10**, 1769–1786, doi:10.1175/1520-0442(1997)010<1769:ENOLNA>2.0.CO;2.

Hu, Z.-Z., A. Kumar, Y. Xue, and B. Jha, 2014: Why were some La Niñas followed by another La Niña? *Climate Dyn.*, **42**, 1029–1042, doi:10.1007/s00382-013-1917-3.

Jin, F.-F., 1997a: An equatorial ocean recharge paradigm for ENSO. 1. Conceptual model. *J. Atmos. Sci.*, **54**, 811–829, doi:10.1175/1520-0469(1997)054<0811:AEORPF>2.0.CO;2.

——, 1997b: An equatorial ocean recharge paradigm for ENSO. Part II: A stripped-down coupled model. *J. Atmos. Sci.*, **54**, 830–847, doi:10.1175/1520-0469(1997)054<0830:AEORPF>2.0.CO;2.

——, and S. I. An, 1999: Thermocline and zonal advective feedbacks within the equatorial ocean recharge oscillator model for ENSO. *Geophys. Res. Lett.*, **26**, 2989–2992, doi:10.1029/1999GL002297.

Kalnay, E., and Coauthors, 1996: The NCEP/NCAR 40-Year Reanalysis Project. *Bull. Amer. Meteor. Soc.*, **77**, 437–471, doi:10.1175/1520-0477(1996)077<0437:TNYRP>2.0.CO;2.

Kistler, R., and Coauthors, 2001: The NCEP–NCAR 50-Year Reanalysis: Monthly means CD-ROM and documentation. *Bull. Amer. Meteor. Soc.*, **82**, 247–267, doi:10.1175/1520-0477(2001)082<0247:TNNYRM>2.3.CO;2.

Kug, J.-S., and I.-S. Kang, 2006: Interactive feedback between ENSO and the Indian Ocean. *J. Climate*, **19**, 1784–1801, doi:10.1175/JCLI3660.1.

Kumar, A., and Z.-Z. Hu, 2014: Interannual and interdecadal variability of ocean temperature along the equatorial Pacific in conjunction with ENSO. *Climate Dyn.*, **42**, 1243–1258, doi:10.1007/s00382-013-1721-0.

Larkin, N. K., and D. E. Harrison, 2002: ENSO warm (El Niño) and cold (La Niña) event life cycles: Ocean surface anomaly patterns, their symmetries, asymmetries, and implications. *J. Climate*, **15**, 1118–1140, doi:10.1175/1520-0442(2002)015<1118:EWENOA>2.0.CO;2.

Lengaigne, M., J. P. Boulanger, C. Menkes, and H. Spencer, 2006: Influence of the seasonal cycle on the termination of El Niño events in a coupled general circulation model. *J. Climate*, **19**, 1850–1868, doi:10.1175/JCLI3706.1.

Li, T., 1997: Phase transition of the El Niño–Southern Oscillation: A stationary SST mode. *J. Atmos. Sci.*, **54**, 2872–2887, doi:10.1175/1520-0469(1997)054<2872:PTOTEN>2.0.CO;2.

Mantua, N. J., and D. S. Battisti, 1994: Evidence for the delayed oscillator mechanism for ENSO—The ''observed'' oceanic Kelvin mode in the far western Pacific. *J. Phys. Oceanogr.*, **24**, 691–699, doi:10.1175/1520-0485(1994)024<0691:EFTDOM>2.0.CO;2.

McPhaden, M. J., and X. Yu, 1999: Equatorial waves and the 1997–98 El Niño. *Geophys. Res. Lett.*, **26**, 2961–2964, doi:10.1029/1999GL004901.

Meinen, C. S., and M. J. McPhaden, 2000: Observations of warm water volume changes in the equatorial Pacific and their relationship to El Niño and La Niña. *J. Climate*, **13**, 3551–3559, doi:10.1175/1520-0442(2000)013<3551:OOWWVC>2.0.CO;2.

Nagura, M., K. Ando, and K. Mizuno, 2008: Pausing of the ENSO cycle: A case study from 1998 to 2002. *J. Climate*, **21**, 342–363, doi:10.1175/2007JCLI1765.1.

Ohba, M., and H. Ueda, 2009: Role of nonlinear atmospheric response to SST on the asymmetric transition process of ENSO. *J. Climate*, **22**, 177–192, doi:10.1175/2008JCLI2334.1.

——, and M. Watanabe, 2012: Role of the Indo-Pacific interbasin coupling in predicting asymmetric ENSO transition and duration. *J. Climate*, **25**, 3321–3335, doi:10.1175/JCLI-D-11-00409.1.

Okumura, Y. M., and C. Deser, 2010: Asymmetry in the duration of El Niño and La Niña. *J. Climate*, **23**, 5826–5843, doi:10.1175/2010JCLI3592.1.

——, M. Ohba, C. Deser, and H. Ueda, 2011: A proposed mechanism for the asymmetric duration of El Niño and La Niña. *J. Climate*, **24**, 3822–3829, doi:10.1175/2011JCLI3999.1.

Picaut, J., F. Masia, and Y. du Penhoat, 1997: An advective–reflective conceptual model for the oscillatory nature of the ENSO. *Science*, **277**, 663–666, doi:10.1126/science.277.5326.663.

Rayner, N. A., D. E. Parker, E. B. Horton, C. K. Folland, L. V. Alexander, D. P. Rowell, E. C. Kent, and A. Kaplan, 2003: Global analyses of sea surface temperature, sea ice, and night marine air temperature since the late nineteenth century. *J. Geophys. Res.*, **108**, 4407, doi:10.1029/2002JD002670.

Ren, H. L., and F.-F. Jin, 2013: Recharge oscillator mechanisms in two types of ENSO. *J. Climate*, **26**, 6506–6523, doi:10.1175/JCLI-D-12-00601.1.

Schneider, E. K., B. Huang, and J. Shukla, 1995: Ocean wave dynamics and El Niño. *J. Climate*, **8**, 2415–2439, doi:10.1175/1520-0442(1995)008<2415:OWDAEN>2.0.CO;2.

Spencer, H., 2004: Role of the atmosphere in seasonal phase locking of El Niño. *Geophys. Res. Lett.*, **31**, L24104, doi:10.1029/2004GL021619.

Stuecker, M. F., A. Timmermann, F.-F. Jin, S. McGregor, and H. L. Ren, 2013: A combination mode of the annual cycle and the El Niño/Southern Oscillation. *Nat. Geosci.*, **6**, 540–544, doi:10.1038/ngeo1826.

Su, J., R. Zhang, T. Li, X. Rong, J.-S. Kug, and C.-C. Hong, 2010: Causes of the El Niño and La Niña amplitude asymmetry in the equatorial eastern Pacific. *J. Climate*, **23**, 605–617, doi:10.1175/2009JCLI2894.1.

Suarez, M. J., and P. S. Schopf, 1988: A delayed action oscillator for ENSO. *J. Atmos. Sci.*, **45**, 3283–3287, doi:10.1175/1520-0469(1988)045<3283:ADAOFE>2.0.CO;2.

Vecchi, G. A., and D. E. Harrison, 2003: On the termination of the 2002–03 El Niño event. *Geophys. Res. Lett.*, **30**, 1964, doi:10.1029/2003GL017564.

Wang, C., 2001: A unified oscillator model for the El Niño–Southern Oscillation. *J. Climate*, **14**, 98–115, doi:10.1175/1520-0442(2001)014<0098:AUOMFT>2.0.CO;2.

——, R. H. Weisberg, and J. I. Virmani, 1999: Western Pacific interannual variability associated with El Niño–Southern Oscillation. *J. Geophys. Res.*, **104**, 5131–5149, doi:10.1029/1998JC900090.

Weisberg, R. H., and C. Wang, 1997: A western Pacific oscillator paradigm for the El Niño–Southern Oscillation. *Geophys. Res. Lett.*, **24**, 779–782, doi:10.1029/97GL00689.

Wyrtki, K., 1985: El Niño—The dynamic response of the equatorial Pacific Ocean to atmospheric forcing. *J. Phys. Oceanogr.*, **5**, 572–584, doi:10.1175/1520-0485(1975)005<0572:ENTDRO>2.0.CO;2.

Zang, X., L.-L. Fu, and C. Wunsch, 2002: Observed reflectivity of the western boundary of the equatorial Pacific Ocean. *J. Geophys. Res.*, **107**, 3150, doi:10.1029/2000JC000719.

Zhang, W., H. Li, F.-F. Jin, M. F. Stuecker, A. G. Turner, and N. P. Klingaman, 2015: The annual-cycle modulation of meridional asymmetry in ENSO's atmospheric response and its dependence on ENSO zonal structure. *J. Climate*, **28**, 5795–5812, doi:10.1175/JCLI-D-14-00724.1.